Faculty of Medical and Health Sciences, University of Poonch Rawalakot
Journal of Pharma and Biomedics
ISSN: 3007-1984(online), 3007-1976 (Print)
https://www.jpbsci.com/index.php/jpbs

Biosynthesis, Characterization and Antibacterial Activity of Iron Oxide Nano-particles

Muhammad Aakash[1], Maria Anwar[1], Minahil Zareen[1], Attia Falak[2], Samyyia Abrar[1]

[1] Department of Biological Sciences, The Superior University, Lahore, Pakistan.
[2] Department of Physics, University of the Punjab, Lahore, Pakistan.

Received: May 22, 2025; Revised: June 27, 2025; Accepted: June 30, 2025

A B S T R A C T

Post-burn infections caused by multidrug-resistant (MDR) bacteria have become a serious global health concern due to limited treatment options. To address this, researchers are turning to green synthesis of metal oxide nanoparticles—a safe, eco-friendly, cost-effective, and less toxic alternative to conventional physical and chemical methods. Nanoparticles synthesized through green routes avoid the need for extreme conditions, toxic chemicals, or external stabilizers, making them especially suitable for biomedical applications. In this study, iron oxide nanoparticles were synthesized using leaf extracts of *Aloe barbadensis*, *Allium sativum*, and *Mentha longifolia*, with ferric chloride ($FeCl_3 \cdot 6H_2O$) as the precursor. Characterization techniques such as UV-visible spectroscopy, SEM, XRD, and FTIR confirmed successful nanoparticle synthesis. UV-Vis peaks (200–400 nm) indicated nanoparticle formation, XRD confirmed crystalline phases (magnetite, hematite, mag-hematite), and FTIR revealed functional groups (O–H, C=O, C≡C) involved in stabilization. SEM showed particle shapes ranging from spherical to cubic and irregular. The synthesized iron oxide nanoparticles demonstrated strong antibacterial activity against MDR gram-negative strains; *Acinetobacter baumannii*, *Pseudomonas aeruginosa*, and *E. coli* with significant zones of inhibition.

Keywords: Post-burn infections, *Aloe barbadensis*, *Allium sativum*, Iron oxide nanoparticles.

Corresponding Author: Samyyia Abrar
Email: samyyia.abrar@superior.edu.pk

INTRODUCTION

The burn infection is one of the significant health challenge in worldwide and infection is one of the prevalent and serious issue in those patient who have sustainable wounds. The infected wound may be a potential source of spreading of antibiotic resistant micro-organisms [1]. Despite in modern advances, the infection and sepsis are the primary cause of death after burns. The main factor is to determine the results of colonization of wound by multi-drug resistant bacteria. This situation is problematic due to insufficient anti-biotic treatment [2]. The underlying tissue of chronic wounds, which persist due to exposure to factors such as bleeding, osteomyelitis, septicemia, and the external environment, significantly raises the mortality rate in patients with chronic burn wounds. Burn wounds also lead to various other complications, including mental health issues, which diminish the quality of life and increase medical costs for patients [1]. Burn patients face an elevated risk of infection due to factors such as the use of catheters for urinary and venous access, arterial lines, tracheal tubes and extended hospital stays [1].

Due to overuse, self-medication, random prescribing of inappropriate medications and prolonged antibiotics use, bacteria have developed drug resistance [3]. Due to overuse and under-use of antibiotics multiple drug resistant in clinical pathogenic bacteria are globally growing and

resulting in one or other multiple drug resistant bacteria [4]. Multi-drug resistant bacteria are critical threat to burn patients that have increased different challenge for medical services. These bacteria are *Proteus pseudomonas, Stephylococcus aureus, Acinetobacter baumannii, Stenotrophomonas maltophilia* [1]. According to WHO carbapanem resistant *Acinetobacter baumannii* has been one of the main concern for the last 10-years due to risk of anti-biotic resistance [5]. *Acinetobacter baumannii* is a non-motile, gram negative bacterium, coccobacillus, non-fermented lactose when grown on MaConkey's agar and strict aerobic, catalase positive and oxidase negative. [3]. Hence, we do not have any antibiotics available for Carbapenem resistant *Acinetobacter baumannii* (CRAB). [6]. Antibacterial activity of many nano-particles including Silver nitrate, Tin oxide, Zinc oxide have already been reported with promising results. But these nano-particles have been synthesized from chemical sources [7].

Synthesis of nano-particles by chemical methods such as element lowering include the use of harmful compounds, creation of toxic by-products and also harmful effects through precursor compounds. So, it is important to acquire fresh non-toxic and environmental friendly procedure for nano-particles synthesis [8, 9]. Therefore, to solve this issue, green chemistry research in nano-particles has recently emerged as a primary focus and as a result many researchers were started to use green chemistry and bio-process to synthesize nano-particles that was reliable, bio-compatible, no use of harmful compounds, cheap and environmental friendly [10, 11].

The current study was planned with research objective including sample collection and bio-synthesis of Iron oxide nano-particles, characterization of bio-synthesized Iron oxide nano-particles and to evaluate antibacterial activity of characterized Iron oxide nano-particles.

METHODOLOGY

Fresh leaves of *Aloe barbadensis* were collected from a botanical garden, while *Mentha longifolia* and *Allium sativum* were sourced from local markets in Pakistan. After thorough washing with distilled water, Aloe leaves were sun-dried for 2–3 days, and Mentha leaves were air-dried for 1–2 days. The dried samples were finely ground, yielding 30 grams of powder from each plant. For iron oxide (Fe_2O_3) nanoparticle synthesis, a 0.1 M solution of ferric chloride hexahydrate ($FeCl_3•6H_2O$) was mixed with plant extracts in a 1:1 ratio and heated at 80°C for 20 minutes, triggering visible color changes indicative of nanoparticle formation. The mixture was then subjected to microwave irradiation at 900W for 18–20 minutes. Post-synthesis, nanoparticles were centrifuged, washed with ethanol, filtered, and dried either under vacuum or in an oven. An additional preparation involved dissolving 10.543 g of $FeCl_3•6H_2O$ in ethanol, followed by the addition of 0.15 g plant extract to ensure proper dispersion. Characterization techniques included FT-IR (for functional group identification), XRD (for crystal structure and size), UV-Vis spectroscopy (confirming surface plasmon resonance), and SEM (for morphology analysis using ImageJ software).

The antibacterial efficacy of the synthesized Fe_2O_3 nanoparticles was tested against multidrug-resistant (MDR) strains of *Escherichia coli*, *Pseudomonas aeruginosa*, and *Acinetobacter baumannii*, obtained from the University of the Punjab. These bacteria, resistant to β-lactams, cephalosporins, and carbapenems, were cultured on MacConkey agar and adjusted to a 0.5 McFarland standard. Crude plant extracts (0.125–1 mg/mL) and Fe_2O_3 nanoparticle suspensions (100 µL) were applied to wells on Mueller Hinton agar plates inoculated with the bacterial strains. Following 18–24 hours of incubation at 37°C, zones of inhibition were measured. The nanoparticles demonstrated promising antibacterial activity, indicating their potential as alternative agents in combating totally drug-resistant pathogens through green, plant-mediated synthesis.

RESULTS

The synthesized iron oxide nanoparticles were characterized using Fourier Transform Infrared Spectroscopy (FTIR), UV-Visible Spectroscopy, X-ray Diffraction (XRD), and Scanning Electron Microscopy (SEM). UV-Vis spectroscopy was carried out using a dual-beam spectrophotometer (200–800 nm), FTIR analysis was performed in the range of 400–4000 cm^{-1} using Opus software, SEM analyzed surface morphology, and XRD determined the crystalline structure of the nanoparticles. FTIR analysis of iron oxide nanoparticles synthesized using *Aloe barbadensis* leaf extract showed peaks between 3100–3700 cm^{-1} indicating O–H groups, 1700–1725 cm^{-1} for C=O stretching in carboxylic acids, and 2160 cm^{-1} for C≡C alkynes, which help stabilize the nanoparticles. A peak at 529 cm^{-1} confirmed the formation of magnetite-phase iron oxide nanoparticles (Figure 1).

Mentha *longifolia*

Figure 2 displays the FTIR analysis of iron oxide nanoparticles synthesized using *Mentha longifolia*, showing peaks between 400–4000 cm^{-1}. Broad peaks at 3500–3700 cm^{-1} indicated O–H groups from ethanol and absorbed water, while peaks at 2000–2200 cm^{-1} corresponded to C≡C

stretching of alkynes. Sharp peaks at 1000–1050 cm^{-1} confirmed the presence of C–O groups, and the peak at 553 cm^{-1} indicated successful formation of iron oxide nanoparticles.

Allium sativum

Figure 3 presents the FTIR analysis of iron oxide nanoparticles synthesized using *Allium sativum*, showing peaks between 400–4000 cm^{-1}. Broad peaks at 3500–3700 cm^{-1} indicated O–H stretching from absorbed water and ethanol, aiding in nanoparticle stabilization. Peaks at 1180–1250 cm^{-1} confirmed the presence of C–O–C groups, while a peak around 1600 cm^{-1} indicated C=C aromatic bending.

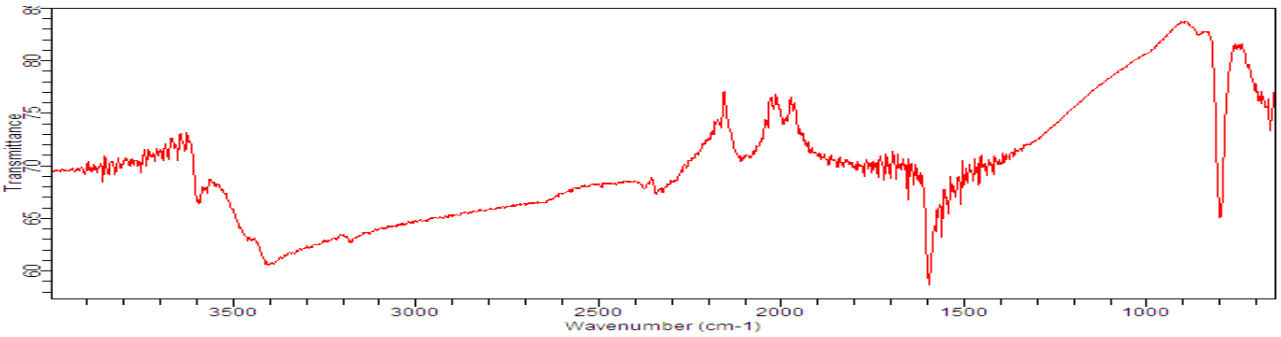

Figure 1: FTIR pattern of Iron oxide nano-particles synthesized by using *Aloe barbadensis* leaf extracts.

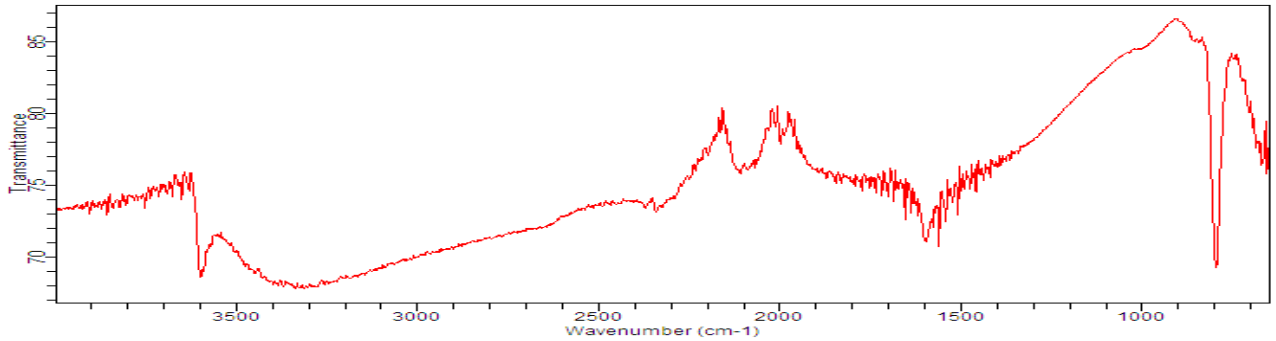

Figure 2: FTIR pattern of Iron oxide nano-particles synthesized by using *Mentha longifolia* leaf extracts.

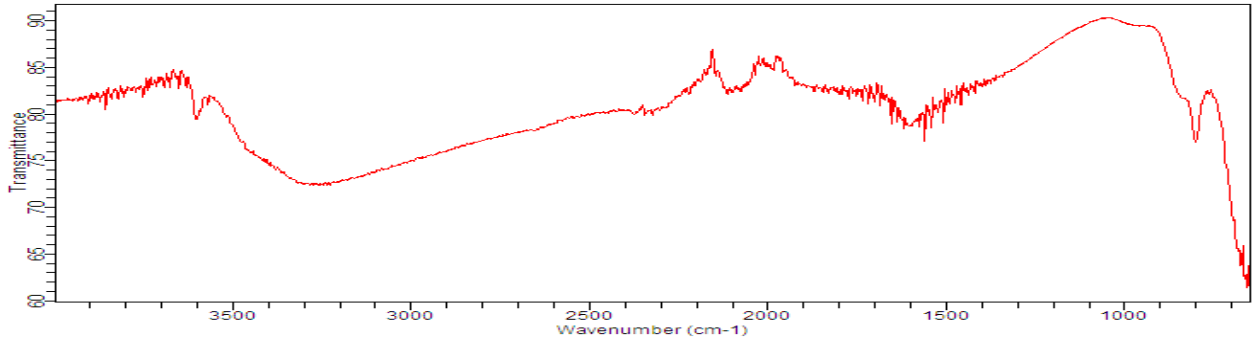

Figure 3: FTIR pattern of Iron oxide nano-particles synthesized by using *Allium sativum* leaf extracts.

UV-visible Spectroscopy

UV-visible spectroscopy measures the absorption of visible and ultraviolet light by a sample. It was used to confirm the synthesis of iron oxide nanoparticles, as these particles absorb UV light and generate distinct absorption spectra.

Aloe barbadensis

Figure 4 displays the UV-visible spectrum of iron oxide nanoparticles synthesized using *Aloe barbadensis* extract. The scan range was 200–800 nm, with notable absorption between 200–400 nm. Sharp peaks at 250–300 nm confirmed the successful formation of iron oxide nanoparticles.

Mentha longifolia

Figure 5 shows the absorption peaks of Iron oxide nano-

particles prepared by using *Mentha longifolia* leaf extracts. The Iron oxide nano-particles were scanned between the ranges of 200nm to 800nm. It can be observed from the figure 4.2.2 that the UV-visible strong peaks were observed between the ranges of 237nm to 405nm that indicated the synthesis of nano-particles of Iron oxide.

Allium sativum

Figure 6 shows the absorption peaks of nano-particles of Iron oxide prepared by using *Allium sativum* leaf extracts. The range of wavelength were between 200nm to 800nm but the sharp and strong absorption peaks of Iron oxide nano-particles synthesized by *Allium sativum* were observed between the range of 250nm to 310nm that confirmed the synthesis of Iron oxide nano-particles. This quite resemble to those previously reported for Iron oxide nano-particles.

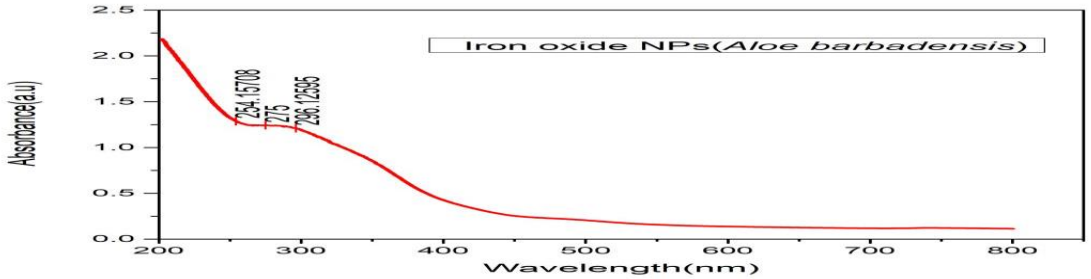

Figure 4: UV-visible absorption spectra of Iron-oxide nano-particles synthesized by using *Aloe barbadensis* leaf extracts.

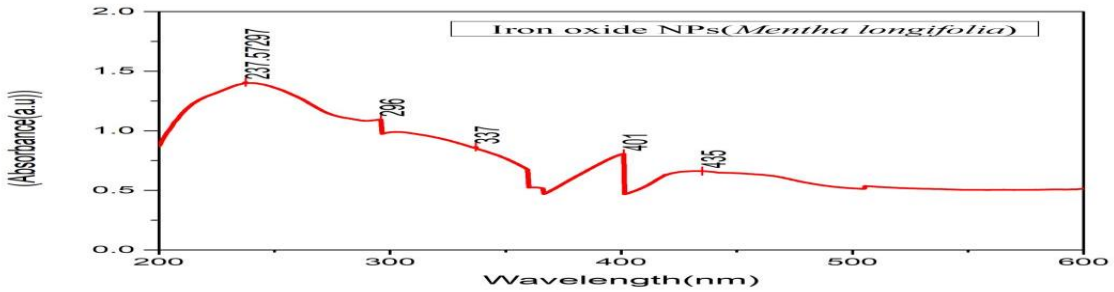

Figure 5: UV-visible absorption spectra of Iron-oxide nano-particles synthesized by using *Mentha longifolia* leaf extracts.

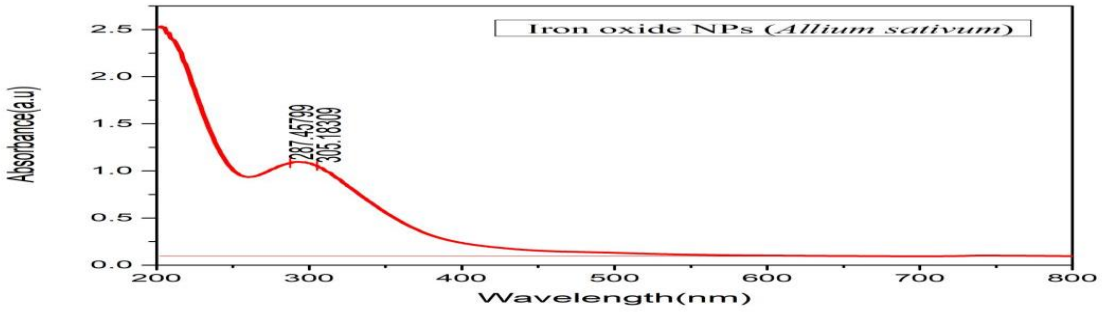

Figure 6: UV-visible absorption spectra of Iron-oxide nano-particles synthesized by using *Allium sativum* leaf extracts.

XRD

X-ray diffraction technique is used to check the assessment of crystallinity of synthesized nano-particles.

Allium sativum

The synthesized iron oxide nanoparticles using *Allium sativum* were characterized by X-ray diffraction. As shown in Figure 7, sharp diffraction peaks appeared at angles 220 (282.5), 240 (280), 260 (311), 340 (317.5), and 560 (295), confirming a well-defined crystalline structure. These distinct reflections indicate the presence of specific

crystallographic planes.

Aloe barbadensis

The synthesized iron oxide nanoparticles using *Aloe barbadensis* were characterized by X-ray diffraction. As shown in Figure 8, sharp diffraction peaks appeared at angles 160 (301), 260 (325), 340 (325), and 560 (311), indicating a crystalline structure. The distinct peak positions suggest the formation of magnetite-phase iron oxide, as opposed to amorphous forms, which typically display broad, diffuse patterns.

Mentha longifolia

The synthesized iron oxide nanoparticles using *Mentha longifolia* were characterized by X-ray diffraction. As shown in Figure 9, diffraction peaks at 260 (302.4), 350 (311), 380 (303), and 550 (312) confirm a crystalline structure with regular atomic arrangement. These peak positions indicate the formation of hematite-phase iron oxide rather than magnetite.

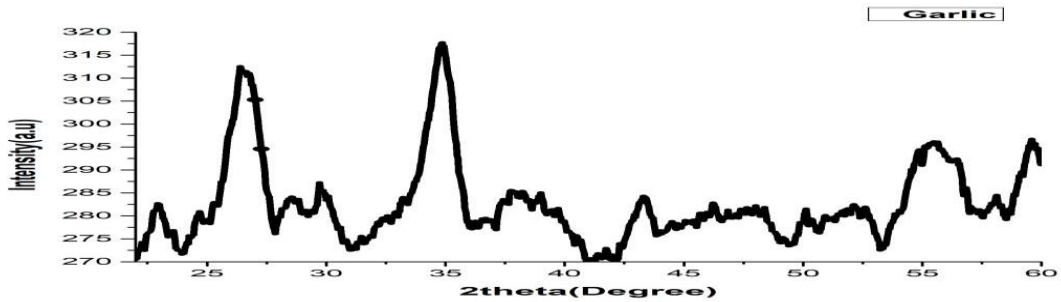

Figure 7: XRD diffraction of Iron-Oxide nano-particles synthesized by using *Allium sativum* leaf extracts.

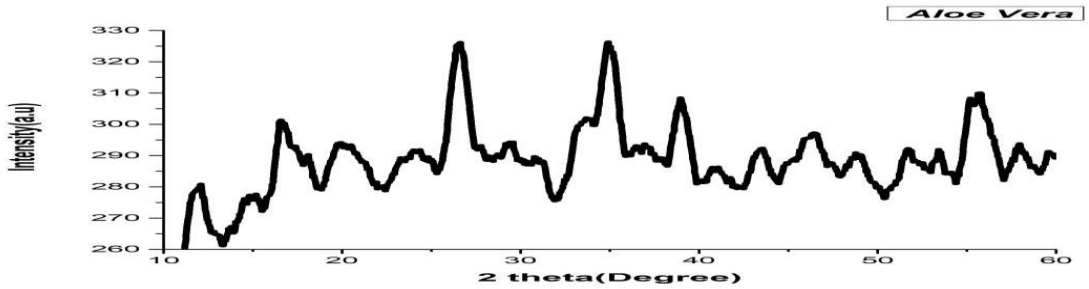

Figure 8: XRD diffraction of Iron-Oxide nano-particles synthesized by using *Aloe barbadensis* leaf extracts.

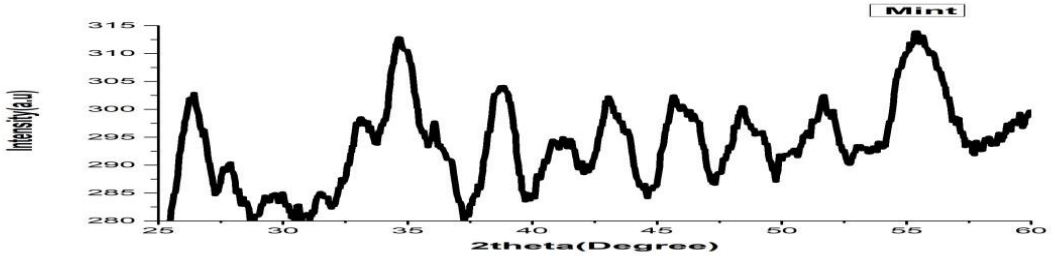

Figure 9: XRD diffraction of Iron-Oxide nano-particles synthesized by using *Mentha longifolia* leaf extracts.

Scanning electron microscopy

The topography or morphological structure of Iron oxide nano-particles was analyzed by using scanning electron microscope at different magnifications of the instrument.

***Aloe* barbadensis**

Figures 10a and 10b show the SEM analysis of iron oxide nanoparticles synthesized using *Aloe barbadensis*. The particles, examined using SEM (JSM-6490) at various magnifications, were mostly clustered with an average size of 90–92 nm. The images reveal that the nanoparticles had relatively uniform size and shape, with most being spherical or cubic, while a few showed irregular form.

Allium sativum

Figures 11a and 11b show the SEM images of iron oxide

nanoparticles synthesized using *Allium sativum*. The analysis revealed that the nanoparticles exhibited both spherical and cubical shapes with some agglomeration.The particle sizes ranged from 24 nm to 123 nm, with an average size of approximately 73 nm. The increase in size for some particles was due to clustering and surface aggregation.

Mentha longifolia

Figures 12a and 12b present the SEM images of iron oxide nanoparticles synthesized using *Mentha longifolia*. At higher magnification, the nanoparticles appeared rough and porous due to aggregation, with irregular and distorted elliptical shapes. At lower magnification, smoother particles were observed. The particle size ranged from 48 nm to 77 nm, with an average size of approximately 64 nm, indicating relatively uniform nanoscale distribution.

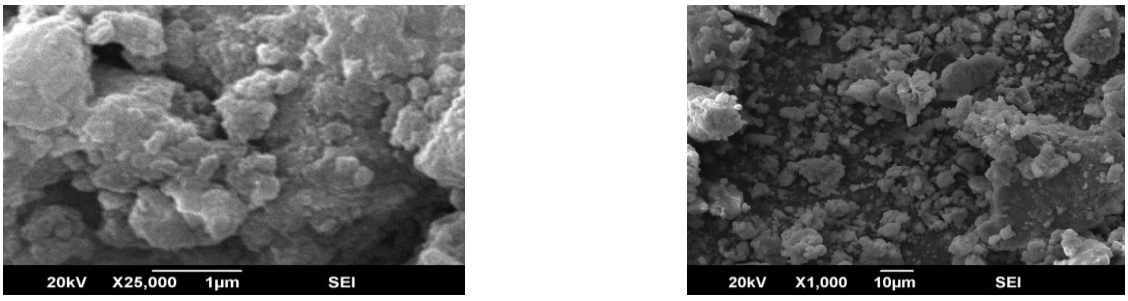

Figure 10: SEM analysis of Iron oxide nano-particles synthesized by using *Aloe barbadensis* leaf extracts at different magnifications, scales: a) 1µm and b) 10µm.

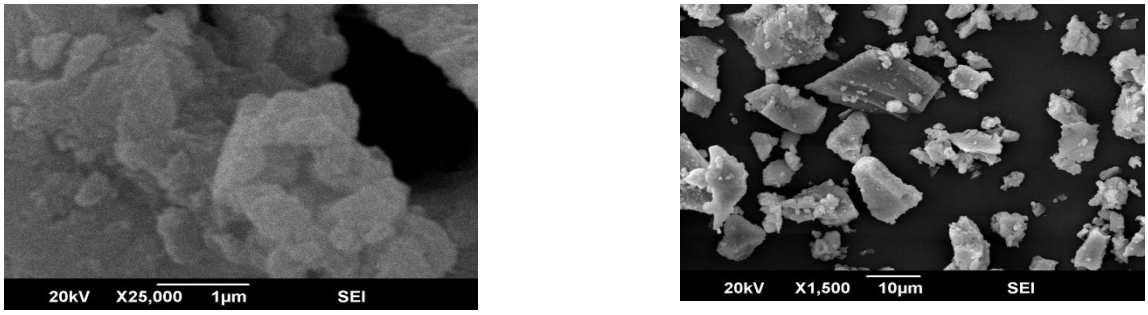

Figure 11: SEM analysis of Iron oxide nano-particles synthesized by using *Allium sativum* leaf extracts at different magnifications, scales: a) 1µm and b) 10µms.

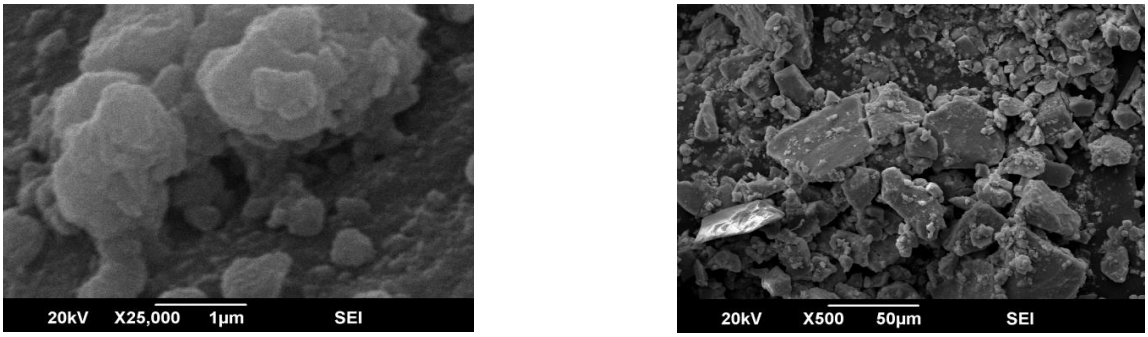

Figure 12: SEM analysis of Iron oxide nano-particles synthesized by using *Mentha longifolia* leaf extracts at different magnifications, scales: a) 1µm and b) 50µm.

Antibacterial activity

Antibacterial Activity of Iron Oxide Nanoparticles against MDR at Different Concentrations

The well diffusion assay was used to evaluate the antibacterial potential of iron oxide nanoparticles synthesized using *Aloe barbadensis*, *Mentha longifolia*, and *Allium sativum* leaf extracts. These nanoparticles were tested against multidrug-resistant strains of *Acinetobacter baumannii*, *E. coli*, and *Pseudomonas aeruginosa*, showing effective antibacterial activity

across all tested pathogens.

Zone of Inhibition of Iron Oxide Nanoparticles Synthesized Using *Mentha longifolia* Leaf Extract

Ascorbic acid (positive control) produced inhibition zones of 12 mm (*P. aeruginosa*), 10 mm (*A. baumannii*), and 12 mm (*E. coli*). Nanoparticles from *Mentha longifolia* showed the highest activity in D1 against *P. aeruginosa* and *E. coli* (12 mm), followed by *A. baumannii* (10 mm). In D2, the maximum inhibition was against *E. coli* (11 mm), while in D3 and D4, inhibition zones progressively decreased, with *E. coli* consistently showing higher sensitivity. Full details are illustrated in Table 1 and figure 13.

Table 1: Zone of inhibition of Fe_2O_3 NPs synthesized by using *Mentha longifolia* leaves extracts.

Bacterial Pathogens	Zone of Inhibition in mm					
	-ve control	Ascorbic acid (+ve control)	D1 (01 mg/ml)	D2 (0.5 mg/ml)	D3 (0.25 mg/ml)	D4 (0.125 mg/ml)
Pseudomonas aeruginosa	0	12	12	10	8	7
E.coli	0	12	12	11	10	8
Acinetobacter baumannii	0	10	10	10	8	8

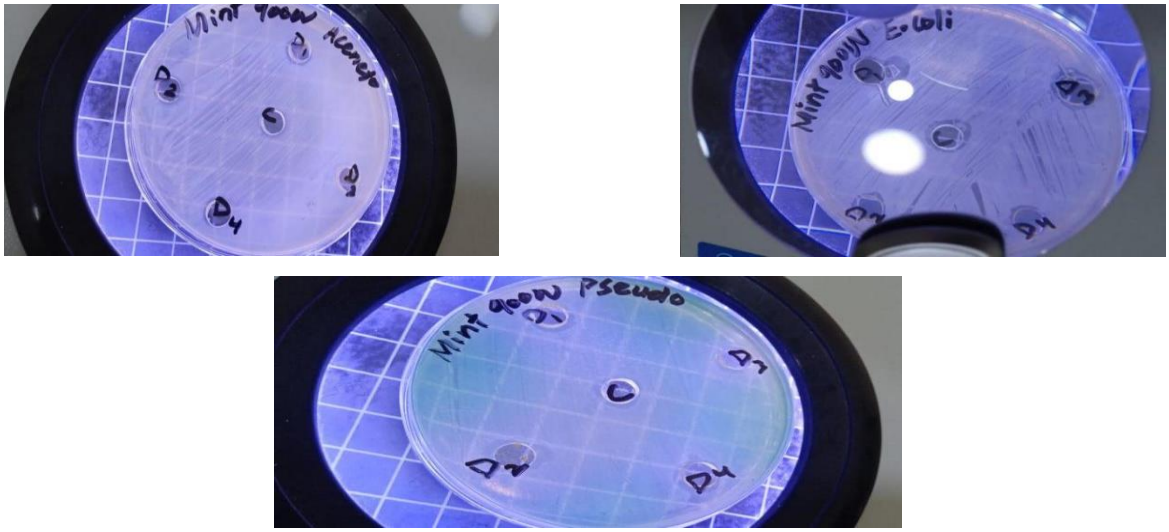

Figure 13: Antibacterial activity of synthesized Iron oxide nano-particles by using *Mentha longifolia* leaves extracts against MDR isolates.

Zone of Inhibition of Iron oxide nano-particles synthesized using *Allium sativum* leaves extract

Ascorbic acid (positive control) produced a uniform inhibition zone of 12 mm against *Pseudomonas aeruginosa*, *Acinetobacter baumannii*, and *E. coli*, as shown in Figure 14 and Table 2. Iron oxide nanoparticles synthesized from *Allium sativum* leaf extract showed the highest inhibition in D1 against *P. aeruginosa* and *E. coli* (12 mm), followed by *A. baumannii* (10 mm). In D2, inhibition zones slightly decreased, with *P. aeruginosa* and *E. coli* at 10 mm and *A. baumannii* at 9 mm. D3 and D4 showed further reductions, with the lowest inhibition in D4: 8 mm (*P. aeruginosa*), 7 mm (*A. baumannii*), and 6 mm (*E. coli*).

Zone of Inhibition of Iron oxide nano-particles synthesized using *Aloe barbadensis* leaves extract

Ascorbic acid (positive control) showed a consistent inhibition zone of 12 mm against *Pseudomonas aeruginosa*, *Acinetobacter baumannii*, and *E. coli*, as shown in Figure 15 and Table 3. Iron oxide nanoparticles synthesized from *Aloe barbadensis* demonstrated the highest antibacterial activity in D1, with *A. baumannii* (20 mm), followed by *P. aeruginosa* (13 mm) and *E. coli* (10 mm). In D2, inhibition zones were 16 mm (*A. baumannii*), 14 mm (*P. aeruginosa*), and 9 mm (*E. coli*). Activity decreased in D3 and D4, with the lowest zones in D4: 10 mm (*A. baumannii*), 8 mm (*P. aeruginosa*), and 6 mm (*E. coli*).

Table2: Zone of inhibition of Iron oxide nano-particles synthesized using *Aloe barbadensis* leaves extracts.

Bacterial Pathogens	Zone of Inhibition in mm					
	-ve control	Ascorbic acid (+ve control)	D1 (1 mg/ml)	D2 (0.5 mg/ml)	D3 (0.25 mg/ml)	D4 (0.125 mg/ml)
Pseudomonas aeruginosa	0	12	13	14	12	8
E.coli	0	12	10	9	8	6
Acinetobacter baumannii	0	12	20	16	12	10

Figure 14: Antibacterial activity of synthesized Iron oxide nano-particles by using *Allium sativum* leaves extracts against MDR isolates.

Table3: Zone of inhibition of Iron oxide nano-particles synthesized using *Aloe barbadensis* leaves extracts.

Bacterial Pathogens	Zone of Inhibition in mm					
	-ve control	Ascorbic acid (+ve control)	D1 (1 mg/ml)	D2 (0.5 mg/ml)	D3 (0.25 mg/ml)	D4 (0.125 mg/ml)
Pseudomonas aeruginosa	0	12	13	14	12	8
E.coli	0	12	10	9	8	6
Acinetobacter baumannii	0	12	20	16	12	10

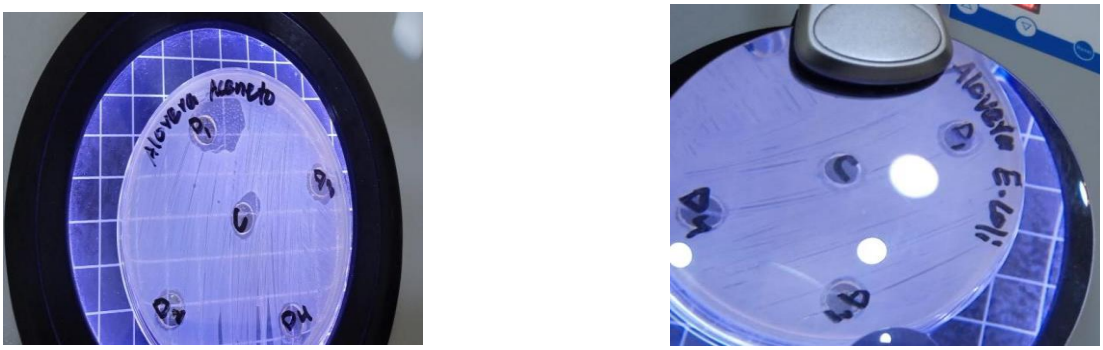

Figure 15: Antibacterial activity of synthesized Iron oxide nano-particles by using *Aloe barbadensis* leaves extracts against MDR isolates.

DISCUSSION

This study aimed to synthesize iron oxide (Fe_2O_3) nanoparticles using leaf extracts from *Aloe barbadensis*, *Allium sativum*, and *Mentha longifolia*, and to evaluate their antibacterial activity against multidrug-resistant (MDR) bacteria responsible for post-burn infections. The nanoparticles were produced via green synthesis using ferric chloride as a precursor and plant extracts as reducing and stabilizing agents. Characterization through FTIR, UV-Vis, XRD, and SEM confirmed the presence of functional groups, crystalline structure, and nanoparticle morphology, with particle sizes ranging from 24 to 93 nm. Nanoparticles from *Aloe barbadensis* showed magnetite characteristics, while those from *Mentha* and *Allium* indicated hematite forms.

Antibacterial testing revealed that the synthesized nanoparticles had strong inhibitory effects against MDR bacteria, including *Escherichia coli*, *Pseudomonas*

aeruginosa, and *Acinetobacter baumannii*, whereas crude plant extracts showed no effect. The enhanced activity is likely due to the nanoparticles' small size and large surface area, enabling effective disruption of bacterial membranes. These findings highlight the promise of green-synthesized iron oxide nanoparticles as alternative treatments for antibiotic-resistant infections, particularly in post-burn cases. Further in vivo studies are recommended to explore their clinical applications.

CONCLUSION

In this study, iron oxide nanoparticles were synthesized using green chemistry with leaf extracts of *Aloe barbadensis*, *Allium sativum*, and *Mentha longifolia*. This eco-friendly, low-cost, and efficient method avoids the use of toxic chemicals and yields nanoparticles with enhanced antimicrobial properties and minimal toxicity to human cells. The synthesis process is influenced by factors such as temperature, reaction time, and salt concentration, and is simple to perform in a laboratory setting without causing environmental pollution.

The synthesized nanoparticles were characterized using UV-Vis spectroscopy, FTIR, XRD, and SEM to determine their shape, size, and surface morphology. Their antimicrobial activity was tested against multidrug-resistant (MDR) bacteria including *Acinetobacter baumannii*, *Pseudomonas aeruginosa*, and *E. coli*. The nanoparticles showed strong antibacterial effects by damaging bacterial cell walls and inhibiting growth, demonstrating large zones of inhibition. These findings suggest that green-synthesized iron oxide nanoparticles hold promise as alternative treatment agents for MDR bacterial infection.

REFERENCES

1. Hemmati J, Azizi M, Asghari B, Arabestani MR. Multidrug-Resistant Pathogens in Burn Wound, Prevention, Diagnosis, and Therapeutic Approaches (Conventional Antimicrobials and Nanoparticles). Canadian Journal of Infectious Diseases and Medical Microbiology. 2023;2023(1):8854311.
2. Vinaik R, Barayan D, Shahrokhi S, Jeschke MG. Management and prevention of drug resistant infections in burn patients. Expert review of anti-infective therapy. 2019;17(8):607-19.
3. Abdulsada FM, Hussein NN, Sulaiman GM. Potentials of Iron Oxide Nanoparticles (Fe3O4): As Antioxidant and Alternative Therapeutic Agent Against Common Multidrug-Resistant Microbial Species. Iraqi Journal of Science. 2023;64(6):2759-73.
4. Ahmed B, Syed A, Ali K, Elgorban AM, Khan A, Lee J, et al. Synthesis of gallotannin capped iron oxide nanoparticles and their broad spectrum biological applications. RSC advances. 2021;11(17):9880-93.
5. Zahra N, Zeshan B, Qadri MMA, Ishaq M, Afzal M, Ahmed N. Phenotypic and genotypic evaluation of antibiotic resistance of Acinetobacter baumannii bacteria isolated from surgical intensive care unit patients in Pakistan. Jundishapur Journal of Microbiology. 2021;14(4).
6. Abdulsada FM, Hussein NN, Sulaiman GM, Al Ali A, Alhujaily M. Evaluation of the antibacterial properties of iron oxide, polyethylene glycol, and gentamicin conjugated nanoparticles against some multidrug-resistant bacteria. Journal of Functional Biomaterials. 2022;13(3):138.
7. Khan Y, Sadia H, Ali Shah SZ, Khan MN, Shah AA, Ullah N, et al. Classification, synthetic, and characterization approaches to nanoparticles, and their applications in various fields of nanotechnology: A review. Catalysts. 2022;12(11):1386.
8. Tahir H, Saad M, Attala OA, El-Saoud WA, Attia KA, Jabeen S, et al. Sustainable Synthesis of Iron–Zinc Nanocomposites by Azadirachta indica Leaves Extract for RSM-Optimized Sono-Adsorptive Removal of Crystal Violet Dye. Materials. 2023;16(3):1023.
9. Yilleng T, Samuel N, Stephen D, Akande J, Agendeh Z, Madaki L. Biosynthesis of copper and iron nanoparticles using neem (Azadirachta indica) leaf extract and their anti-bacterial activity. Journal of Applied Sciences and Environmental Management. 2020;24(11):1987-91.
10. Patil YY, Sutar VB, Tiwari AP. Green synthesis of magnetic iron nanoparticles using medicinal plant Tridax procumbens leaf extracts and its application as an antimicrobial agent against E. coli. International Journal of Applied Pharmaceutics. 2020;12:34-9.
11. Jamalia AR, Batoolc M, Asghara SA, Akhterb F, Hussaina F, Khurshidd S. Synthesis of Green Metaloxide Nanoparticles using Aloe-Barbadensis Leaf Extract (Acid Red 28) for Dye Removal Applications. Jurnal Kejuruteraan. 2022;34(5):801-5.